Biophysical *Journal*
Biophysical Letter

Biophysical Society

Spherical Caps in Cell Polarization

Rocky Diegmiller,[1,2] Hadrien Montanelli,[3] Cyrill B. Muratov,[4,*] and Stanislav Y. Shvartsman[1,2,*]
[1]Department of Chemical and Biological Engineering and [2]Lewis-Sigler Institute for Integrative Genomics, Princeton University, Princeton, New Jersey; [3]Department of Applied Physics and Applied Mathematics, Columbia University, New York, New York; and [4]Department of Mathematical Sciences, New Jersey Institute of Technology, Newark, New Jersey

ABSTRACT Intracellular symmetry breaking plays a key role in wide range of biological processes, both in single cells and in multicellular organisms. An important class of symmetry-breaking mechanisms relies on the cytoplasm/membrane redistribution of proteins that can autocatalytically promote their own recruitment to the plasma membrane. We present an analytical construction and a comprehensive parametric analysis of stable localized patterns in a reaction-diffusion model of such a mechanism in a spherical cell. The constructed patterns take the form of high-concentration patches localized into spherical caps, similar to the patterns observed in the studies of symmetry breaking in single cells and early embryos.

Many important processes in cell and developmental biology are controlled by highly nonuniform intracellular distributions of protein concentrations and enzymatic activities (1,2). Examples include polarized patterns of membrane localization observed in studies of mating responses in yeast (3–7) and early embryogenesis in *Caenorhabditis elegans* (8–10). In both cases, patterns take the form of a localized cap on a cell membrane and play an instructive role, leading to the formation of a budding protrusion in yeast and asymmetric localization of cell determinants in the *C. elegans* embryo, respectively.

The formation of such cap-like patterns can rely on autocatalytic membrane recruitment of a diffusible cytoplasmic protein. The molecular and cellular bases for this mechanism have been established in several cases, motivating an impressive number of mathematical models that are being used to explore the quantitative requirements for the formation of robust localized patterns (5,8,11–18). The simplest of such models has a single chemical species that interconverts between membrane and cytoplasmic states (13,14,17). One critical aspect is that self-promoted membrane recruitment can give rise to bistability, whereby the membrane can be in two states with very different levels of accumulated protein. This is the model considered in this Letter (Fig. 1).

In the system under consideration, the species with concentration C moves freely with diffusivity D_C in the cell interior and reversibly binds to the cell membrane. The cell interior and the membrane are denoted by Ω and $\partial\Omega$, respectively. The dissociation-rate constant is denoted by k_d. The membrane-bound species, with surface density B, has diffusivity D_B and promotes its own recruitment to the membrane. This is described by making the forward-binding rate a sigmoidal function of protein concentration at the membrane. The binding rate is modeled as a sum of two terms: the first term describes constitutive binding; the second term reflects autocatalytic recruitment, which follows a Hill-like dependence. These are characterized by the rate constant k_b, constitutive rate β, threshold value Γ, and cooperativity parameter ν. The joint dynamics of the cytoplasmic and membrane species in a spherical cell of radius r is then governed by the following equations:

$$\frac{\partial B}{\partial t} = D_B \nabla^2_{r\mathbb{S}^2} B + k_b \left(\beta + \frac{B^\nu}{B^\nu + \Gamma^\nu}\right) C - k_d B, \qquad (1)$$

$$\frac{\partial C}{\partial t} = D_C \nabla^2 C, \qquad (2)$$

and

$$D_C (\nabla C \cdot \hat{n})\,|_{r\mathbb{S}^2} = -k_b \left(\beta + \frac{B^\nu}{B^\nu + \Gamma^\nu}\right) C + k_d B. \qquad (3)$$

In these equations, $\hat{n}$ is the outward unit normal to $\partial\Omega = r\mathbb{S}^2$, ∇^2 is the spherical Laplacian in Ω, and $\nabla^2_{r\mathbb{S}^2}$ is the Laplace-Beltrami operator on $\partial\Omega$:

$$\nabla^2_{r\mathbb{S}^2} = \frac{1}{r^2 \sin\theta} \frac{\partial}{\partial\theta}\left(\sin\theta \frac{\partial}{\partial\theta}\right) + \frac{1}{r^2 \sin^2\theta} \frac{\partial^2}{\partial\phi^2}, \qquad (4)$$

Submitted April 12, 2018, and accepted for publication May 29, 2018.
*Correspondence: muratov@njit.edu or stas@princeton.edu
Editor: Anatoly Kolomeisky.
https://doi.org/10.1016/j.bpj.2018.05.033

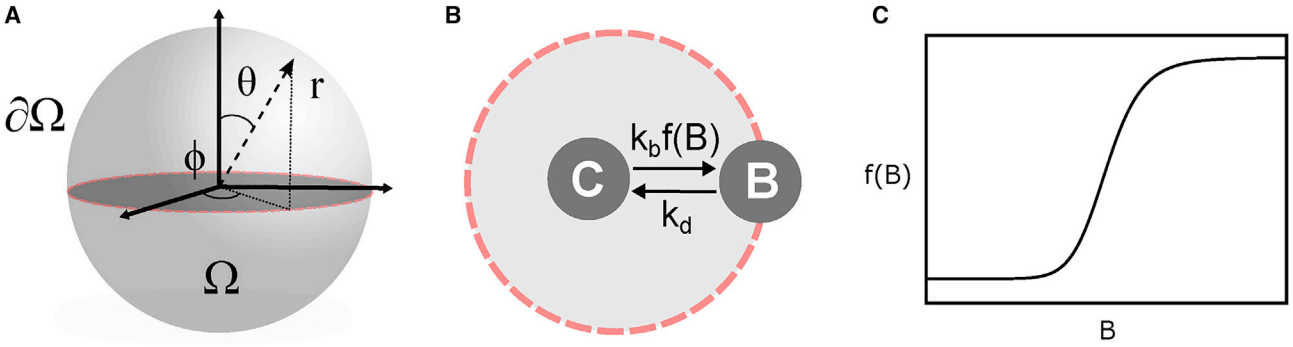

FIGURE 1 (*A*) Schematic of a spherical cell. (*B*) The membrane association and dissociation processes are shown. (*C*) The function modeling the autocatalytic membrane recruitment is shown. To see this figure in color, go online.

where $\theta \in [0, \pi]$ and $\phi \in [0, 2\pi]$ are the angular variables of the standard spherical coordinates.

This model and many of its relatives considered in the context of cell polarization belong to a broad class of reaction-diffusion systems with spatially segregated compartments of different dimensionality (15,18–22). In combination with diffusion on the membrane, autocatalytic membrane recruitment can result in the formation and progressive expansion of a domain with high membrane concentration (11,13–20,23,24). However, it is counteracted by total mass conservation and fast cytoplasmic diffusion (12–14). For a proper choice of model parameters, localized accumulation on the membrane depletes concentration in the cytoplasm and can stabilize the expanding domain, resulting in a stable pattern.

Because the total amount of protein in the system is constant, the membrane and bulk protein concentrations are globally coupled by mass conservation. Although the general phenomenology associated with the formation of localized patterns in globally coupled reaction-diffusion problems is well understood (19,20,23), the number of results in the context of intracellular symmetry breaking is very limited (4,16,24). In fact, all existing analytical results are limited to one-dimensional "cells" and are based on ad hoc descriptions of nonlocal coupling of membrane dynamics by cytoplasmic diffusion (12–14,17,25). Here, we report exact analytical solutions for the spherical cap patterns constructed in the regime of large cytoplasmic diffusion that properly take into account the three-dimensional geometry of the cell.

We start by considering the conservation equation for the total amount of a protein, which is not synthesized or degraded but only redistributed between cytoplasm and membrane (5,12,13):

$$\int_{\Omega} C \, \mathrm{d}V + \int_{\partial\Omega} B \, \mathrm{d}S = \frac{4}{3}\pi r^3 C_0, \tag{5}$$

where C_0 is the total amount of protein in the cell divided by cell volume. Because cytoplasmic diffusivity is typically much larger than membrane diffusivity, the cytoplasmic concentration may be assumed to be uniform throughout the cell (see Supporting Materials and Methods for further discussion):

$$C = C_0 - \frac{3}{4\pi r^3}\int_{\partial\Omega} B \, \mathrm{d}S. \tag{6}$$

Upon substitution of this expression into Eq. 1, our model is reduced to a single equation for the membrane species (26). This equation is rendered dimensionless by the following transformations: $\tau \equiv k_d t$ and $u \equiv k_d B/(k_b C_0)$. This leads to the following problem for the spatiotemporal dynamics of the dimensionless cell surface concentration, $u = u(\theta, \phi, \tau)$:

$$\frac{\partial u}{\partial \tau} = \delta^2 \nabla^2_{\mathbb{S}^2} u - u + \left(1 - \frac{\alpha}{2\pi}\int_0^{2\pi}\int_0^{\pi} u \sin\theta \, \mathrm{d}\theta \, \mathrm{d}\phi\right)\left(\beta + \frac{u^\nu}{u^\nu + \gamma^\nu}\right). \tag{7}$$

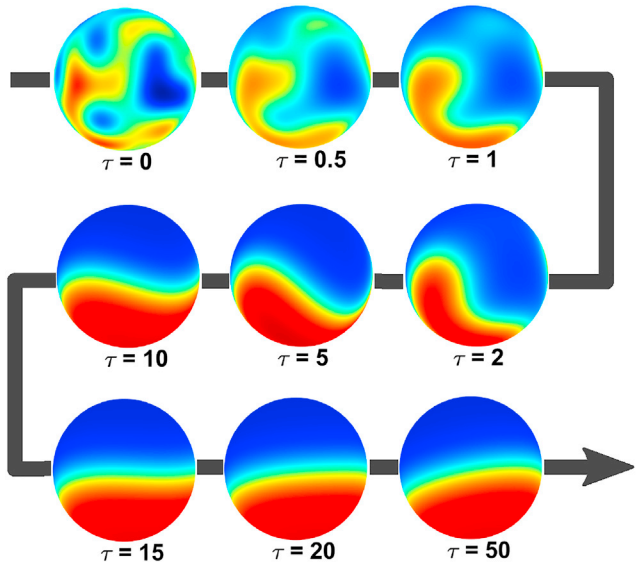

FIGURE 2 Snapshots of cell surface concentration from a representative numerical solution of Eq. 7 with $\alpha = 1, \beta = 0.1, \gamma = 0.3, \delta^2 = 0.05$, and $\nu = 20$. To see this figure in color, go online.

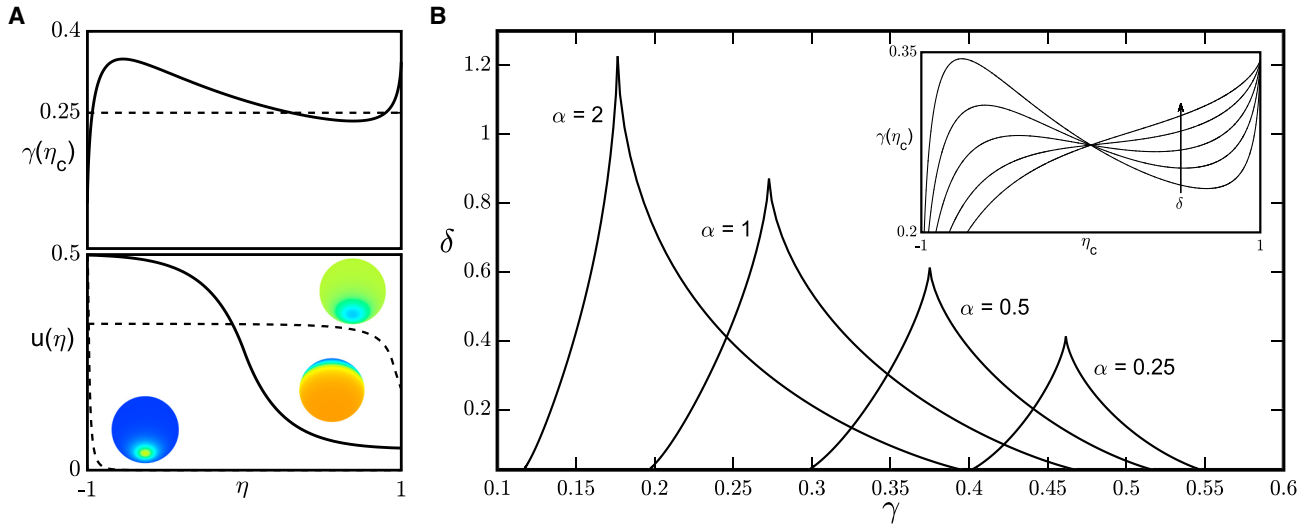

FIGURE 3 (*A*) Construction of spatially nonuniform steady states. The graphical solution of Eq. 11, for $\alpha = 1$, $\beta = 0.1$, $\gamma = 0.25$, and $\delta = 0.3$, reveals three roots (*top panel*), giving rise to three different spatial profiles (*bottom panel*). (*B*) Two-dimensional cuts through the four-dimensional domain of model parameters that support the formation of stable localized patterns for $\beta = 0.1$ are shown. The boundaries of the cusps correspond to the extrema of the $\gamma(\eta_c)$ function; this function becomes monotonic at the tip of the cusp (*inset*). Here, the inset shows $\gamma(\eta_c)$ for $\beta = 0.1$, $\alpha = 1$, and $\delta = \{0.1, 0.25, 0.5, 1, 2\}$. To see this figure in color, go online.

The rescaled problem has five dimensionless groups: ν and β are inherited directly from the original model; $\gamma \equiv k_d\Gamma/(k_bC_0)$ is the dimensionless threshold for the membrane recruitment nonlinearity; $\delta^2 \equiv D_B/(k_dr^2)$ is the ratio of characteristic times for dissociation from the membrane and surface diffusion; and finally, $\alpha \equiv 3k_b/(2k_dr)$ may be interpreted as the ratio of the maximal fluxes to and from the cell membrane and quantifies the strength of the global coupling essential for the formation of localized patterns.

We started our analysis of this problem by solving it numerically using a spectral discretization implemented in the Chebfun package (27,28). In all cases, the system converged to one of two types of behaviors: uniform steady state profiles and nonuniform axisymmetric cap-like patterns. Fig. 2 shows the snapshots from a representative numerical solution that eventually converges to such a pattern. Our numerical experiments indicate that such solitary caps, although placed at different locations on the surface, are the only spatially nonuniform attractors of Eq. 7.

The axial symmetry of the cap-like patterns allows us to reduce the dimensionality of the problem. Without loss of generality, we may place the cap center at the North Pole of the sphere and focus only on the ϕ-independent solutions. Furthermore, when the membrane-recruitment nonlinearity is sharp ($\nu \gg 1$), it can be approximated by the Heaviside function. Using a common coordinate transformation, $\eta = -\cos\theta \in [-1,1]$, we obtain the following ordinary differential equation for the axially symmetric steady state solution $u = \overline{u}(\eta)$:

$$\delta^2 \frac{d}{d\eta}\left[\left(1-\eta^2\right)\frac{d\overline{u}}{d\eta}\right] = \overline{u} - \left(1 - \alpha\int_{-1}^{1}\overline{u}\,d\eta\right) \times \left(\beta + H(\overline{u}-\gamma)\right). \tag{8}$$

This equation is piecewise linear, which greatly simplifies the analysis of localized patterns. One can readily check that this equation may have at most two spatially uniform stable steady states, in which the membrane concentration is either above or below the threshold value:

$$u_- = \frac{\beta}{1+2\alpha\beta} \text{ and } u_+ = \frac{1+\beta}{1+2\alpha(1+\beta)}.$$

In addition to these uniform steady states, we found patterned solutions that correspond to spherical caps. In constructing these solutions, we assumed that they decrease monotonically from $\eta = -1$ to $\eta = 1$, crossing the threshold at some value of the longitudinal coordinate: $\overline{u}(\eta_c) = \gamma$. In other words, the autocatalytic membrane recruitment is "on" for $\eta < \eta_c$ and "off" for $\eta > \eta_c$. As shown in the Supporting Material, such steady states can be found analytically in terms of the Legendre function $P_\mu(\eta)$, where $\mu = (1/2)(\sqrt{1-4\delta^{-2}} - 1)$:

$$\overline{u}(\eta > \eta_c) = (\gamma - \beta k)\frac{P_\mu(\eta)}{P_\mu(\eta_c)} + \beta k \tag{9}$$

and

$$\overline{u}(\eta < \eta_c) = (\gamma - (1+\beta)k)\frac{P_\mu(-\eta)}{P_\mu(-\eta_c)} + (1+\beta)k, \tag{10}$$

where

$$k = \frac{\gamma\left(1+\frac{P'_\mu(\eta_c)}{P'_\mu(-\eta_c)}\frac{P_\mu(-\eta_c)}{P_\mu(\eta_c)}\right)}{1+\beta\left(1+\frac{P'_\mu(\eta_c)}{P'_\mu(-\eta_c)}\frac{P_\mu(-\eta_c)}{P_\mu(\eta_c)}\right)}.$$

To evaluate these expressions, one must find the position η_c where $\overline{u}(\eta_c) = \gamma$. This position can be found from the dimensionless form of the conservation law for the total amount of protein, leading to the following implicit function that relates η_c to the dimensionless parameters of the problem:

$$\gamma = \frac{1+\beta\left(1+\frac{P'_\mu(\eta_c)}{P'_\mu(-\eta_c)}\frac{P_\mu(-\eta_c)}{P_\mu(\eta_c)}\right)}{\left(1+\frac{P'_\mu(\eta_c)}{P'_\mu(-\eta_c)}\frac{P_\mu(-\eta_c)}{P_\mu(\eta_c)}\right)(1+\alpha(1+\eta_c)+2\alpha\beta)}. \tag{11}$$

Graphical analysis of this equation reveals that it can have up to three roots, corresponding to three different values of η_c for which $\overline{u}(\eta_c) = \gamma$ (Fig. 3). Each of these values gives rise to a different spatially nonuniform steady state. In particular, in the biologically significant regime of $\delta \ll 1$, there exists one solution in the form of a large spherical cap, for which

$$\gamma(\eta_c) \simeq \frac{2\beta+1}{2(1+\alpha(2\beta+1+\eta_c))}, \tag{12}$$

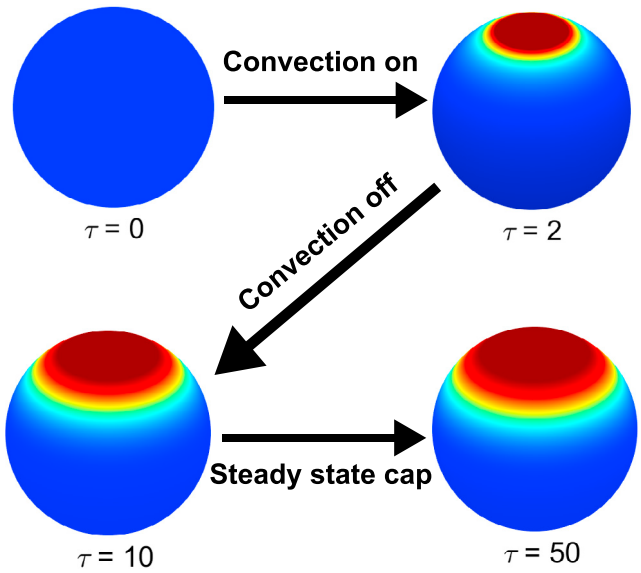

FIGURE 4 Directed control of pattern formation by a transient unidirectional flow. The system starts from a uniform "off" steady state. The flow is from the South to North Pole. $\alpha = 1$, $\beta = 0.1$, $\gamma = 0.35$, and $\delta^2 = 0.05$. See the Supporting Materials and Methods for details. To see this figure in color, go online.

and two small spherical cap solutions, for which $\sqrt{1-\eta_c^2} \sim \delta$ whenever $\gamma \in \left(\frac{2\beta+1}{2(1+2\alpha(\beta+1))}, \frac{2\beta+1}{2(1+2\alpha\beta)}\right)$. Stability analysis of these solutions (see Supporting Materials and Methods) shows that for $\delta \ll 1$, a spherical cap solution is stable if and only if $\alpha > \alpha_c$, where

$$\alpha_c \simeq \frac{\delta}{2(2\beta+1)\left(1-\eta_c^2\right)^{3/2}}. \tag{13}$$

According to this formula, for all δ sufficiently small and γ in the above range, the small-cap solutions are linearly unstable, whereas the large cap is linearly stable. We note that, as expected, the stable solutions constructed analytically above persist in the problem with ν finite, even for $\nu \approx 5$.

Equation 11 may be used to delineate the four-dimensional domain of parameters α, β, γ, and δ that can support states with broken symmetry. Fig. 3 shows a series of two-dimensional cuts through this domain, computed at a constant value of constitutive membrane recruitment and four different strengths of the global coupling parameter. For each of these cuts, the localized patterns exist in a cusp-like region that is characterized by an upper limit for dimensionless surface diffusivity δ. Beyond this value, the right-hand side of Eq. 11 becomes a single-valued function of γ_c (see the *inset* of Fig. 3 *B*), which corresponds to the disappearance of stable patterns. Our analysis also reveals how reducing the strength of global coupling moves the system outside of the domain corresponding to the symmetry-broken stable steady states.

Our results provide insights into the parametric dependence and robustness of the localized patterns. For instance, changes in the cell radius affect two dimensionless groups: the dimensionless-cell-surface diffusivity, $\delta \sim 1/r$, and the strength of global coupling, $\alpha \sim 1/r$. Because the existence of patterned states is promoted by small values of surface diffusivity and strong global coupling, patterned states are realized for an intermediate range of cell sizes (see Fig. S2).

Further research is required to understand how cells can not only form the localized patterns but also direct them to specific positions. Studies in the early *C. elegans* embryo suggest that such control may be provided by cortical flows that transiently localize the diffusible species at a specific location on the cell membrane (1,8,10). Our model can be readily modified to account for such flows. As an illustration, Fig. 4 shows the results of a numerical experiment in which a model cell starts from a steady state in which most of the protein is cytoplasmic. A transient unidirectional flow then creates a region of high membrane concentration, triggering the formation of a self-sustained localized pattern.

An additional layer of control may be provided by variations in the curvature of the cell surface. Our preliminary simulations in spheroid geometries indicate that large spherical cap solutions persist under perturbations of spherical symmetry but at the same time are guided to specific

locations by variations of curvature. Analyzing the effects of such variations, which can be either static or dynamic, should provide additional insights into the mechanisms of intracellular symmetry breaking (1,2).

SUPPORTING MATERIAL

Supporting Materials and Methods and three figures are available at http://www.biophysj.org/biophysj/supplemental/S0006-3495(18)30672-6.

AUTHOR CONTRIBUTIONS

S.Y.S. and C.B.M. designed the research. C.B.M. and R.D. performed analytical and numerical studies. H.M. provided software and numerical analysis.

ACKNOWLEDGMENTS

The authors thank Dr. Mahim Misra for his contributions during the early stages of this work.

This work was supported by funding from the National Science Foundation Science and Technology Center for Emergent Behaviors of Integrated Cellular Systems (CBET-0939511) and National Institutes of Health (R01GM107103). This research was partially supported by the Allen Discovery Center program through The Paul G. Allen Frontiers Group.

SUPPORTING CITATIONS

References (29–36) appear in the Supporting Material.

REFERENCES

1. Mogilner, A., J. Allard, and R. Wollman. 2012. Cell polarity: quantitative modeling as a tool in cell biology. *Science.* 336:175–179.
2. Kim, E. J. Y., E. Korotkevich, and T. Hiiragi. Coordination of cell polarity, mechanics and fate in tissue self-organization. *Trends Cell Biol*. Published online March 28, 2018. https://doi.org/10.1016/j.tcb.2018.02.008.
3. Chiou, J. G., M. K. Balasubramanian, and D. J. Lew. 2017. Cell polarity in yeast. *Annu. Rev. Cell Dev. Biol.* 33:77–101.
4. Giese, W., M. Eigel, …, E. Klipp. 2015. Influence of cell shape, inhomogeneities and diffusion barriers in cell polarization models. *Phys. Biol.* 12:066014.
5. Goryachev, A. B., and A. V. Pokhilko. 2008. Dynamics of Cdc42 network embodies a Turing-type mechanism of yeast cell polarity. *FEBS Lett.* 582:1437–1443.
6. Goryachev, A. B., and M. Leda. 2017. Many roads to symmetry breaking: molecular mechanisms and theoretical models of yeast cell polarity. *Mol. Biol. Cell.* 28:370–380.
7. Klünder, B., T. Freisinger, …, E. Frey. 2013. GDI-mediated cell polarization in yeast provides precise spatial and temporal control of Cdc42 signaling. *PLoS Comput. Biol.* 9:e1003396.
8. Goehring, N. W., P. K. Trong, …, S. W. Grill. 2011. Polarization of PAR proteins by advective triggering of a pattern-forming system. *Science.* 334:1137–1141.
9. Lang, C. F., and E. Munro. 2017. The PAR proteins: from molecular circuits to dynamic self-stabilizing cell polarity. *Development.* 144:3405–3416.
10. Mittasch, M., P. Gross, …, M. Kreysing. 2018. Non-invasive perturbations of intracellular flow reveal physical principles of cell organization. *Nat. Cell Biol.* 20:344–351.
11. Alonso, S., and M. Bär. 2010. Phase separation and bistability in a three-dimensional model for protein domain formation at biomembranes. *Phys. Biol.* 7:046012.
12. Otsuji, M., S. Ishihara, …, S. Kuroda. 2007. A mass conserved reaction-diffusion system captures properties of cell polarity. *PLoS Comput. Biol.* 3:e108.
13. Mori, Y., A. Jilkine, and L. Edelstein-Keshet. 2008. Wave-pinning and cell polarity from a bistable reaction-diffusion system. *Biophys. J.* 94:3684–3697.
14. Mori, Y., A. Jilkine, and L. Edelstein-Keshet. 2011. Asymptotic and bifurcation analysis of wave-pinning in a reaction-diffusion model for cell polarization. *SIAM J. Appl. Math.* 71:1401–1427.
15. Rätz, A., and M. Röger. 2012. Turing instabilities in a mathematical model for signaling networks. *J. Math. Biol.* 65:1215–1244.
16. Rätz, A., and M. Röger. 2013. Symmetry breaking in a bulk-surface reaction-diffusion model for signaling networks. *Nonlinearity.* 27:1805–1827.
17. Trong, P. K., E. M. Nicola, …, S. W. Grill. 2014. Parameter-space topology of models for cell polarity. *New J. Phys.* 16:065009.
18. Anguige, K., and M. Röger. 2017. Global existence for a bulk/surface model for active-transport-induced polarisation in biological cells. *J. Math. Anal. Appl.* 448:213–244.
19. Middya, U., D. Luss, and M. Sheintuch. 1994. Impact of global interaction and symmetry on pattern selection and bifurcation. *J. Chem. Phys.* 101:4688–4696.
20. Pismen, L. M. 1994. Turing patterns and solitary structures under global control. *J. Chem. Phys.* 101:3135–3146.
21. Còsul, N. 1996. On equilibrium solutions of diffusion equations with nonlinear boundary conditions. *Z. Angew. Math. Phys.* 47:194–209.
22. Přibyl, M., C. B. Muratov, and S. Y. Shvartsman. 2003. Long-range signal transmission in autocrine relays. *Biophys. J.* 84:883–896.
23. Battogtokh, D., M. Hildebrand, …, A. Mikhailov. 1997. Nucleation kinetics and global coupling in reaction-diffusion systems. *Phys. Rep.* 288:435–456.
24. Madzvamuse, A., and A. H. W. Chung. 2016. The bulk-surface finite element method for reaction-diffusion systems on stationary volumes. *Finite Elem. Anal. Des.* 108:9–21.
25. Rubinstein, B., B. D. Slaughter, and R. Li. 2012. Weakly nonlinear analysis of symmetry breaking in cell polarity models. *Phys. Biol.* 9:045006.
26. Hale, J. K., and K. Sakamoto. 1989. Shadow systems and attractors in reaction-diffusion equations. *Appl. Anal.* 32:287–303.
27. Driscoll, T. A., N, Hale, and L. N., Trefethen, eds. 2014. Chebfun Guide: Pafnuty Publications, Oxford, UK.
28. Wright, G. B., M. Javed, …, L. N. Trefethen. 2015. Extension of Chebfun to periodic functions. *SIAM J. Sci. Comput.* 37:C554–C573.
29. Abramowitz, M., and I. A. Stegun. 1964. Handbook of Mathematical Functions with Formulas, Graphs, and Mathematical Tables. National Bureau of Standards, Dover, New York.
30. Kerner, B. S., and V. V. Osipov. 1994. Autosolitons. Springer-Science + Business Media, Dordrecht, the Netherlands.
31. Kerner, B. S., and V. V. Osipov. 1978. Long-range signal transmission in autocrine relays. *Sov. Phys. JETP.* 47:874–885.
32. Kerner, B. S., and V. V. Osipov. 1982. Pulsating "heterophase" regions in nonequilibrium systems. *Sov. Phys. JETP.* 56:1275–1282.
33. Muratov, C. B., and V. V. Osipov. 1996. General theory of instabilities for patterns with sharp interfaces in reaction-diffusion systems. *Phys. Rev. E Stat. Phys. Plasmas Fluids Relat. Interdiscip. Topics.* 53:3101–3116.
34. Bose, A., and G. A. Kriegsmann. 1998. Stability of localized structures in non-local reaction-diffusion equations. *Meth. Appl. Anal.* 5:351–366.
35. Muratov, C. B., and V. V. Osipov. 2002. Stability of static spike autosolitons in the Gray-Scott model. *SIAM J. Appl. Math.* 62:1463–1487.
36. Montanelli, H., and Y. Nakatsukasa. 2018. Fourth-order time-stepping for stiff PDEs on the sphere. *SIAM J. Sci. Comput.* 40:A421–A451.

Biophysical Journal, Volume *115*

Supplemental Information

Spherical Caps in Cell Polarization

Rocky Diegmiller, Hadrien Montanelli, Cyrill B. Muratov, and Stanislav Y. Shvartsman

Supporting Material: Spherical caps in cell polarization

Rocky Diegmiller[1], Hadrien Montanelli[2], Cyrill B. Muratov[3], and Stanislav Y. Shvartsman[1]

[1] *Department of Chemical and Biological Engineering and Lewis-Sigler Institute for Integrative Genomics, Princeton University, Princeton, NJ, 08544, USA*

[2] *Department of Applied Physics and Applied Mathematics, Columbia University, New York, NY, 10027, USA*

[3] *Department of Mathematical Sciences, New Jersey Institute of Technology, Newark, NJ, 07102, USA*

Axisymmetric Steady States

In this section, we derive the steady state solutions in the form of axisymmetric caps for a given set of model parameters $(\alpha, \beta, \gamma, \delta)$. Equation (8) in the main text is an ODE that defines $u = \bar{u}(\eta)$ on the surface of the sphere at steady state:

$$0 = \delta^2 \frac{d}{d\eta}\left[(1-\eta^2)\frac{d\bar{u}}{d\eta}\right] + \left(1 - \alpha\int_{-1}^{1} \bar{u}\ \mathrm{d}\eta\right)(\beta + H(\bar{u}-\gamma)) - \bar{u}. \tag{S1}$$

By inspection, this ODE yields two stable uniform solutions $u = u_\pm$ lying below and above the threshold $u = \gamma$, respectively:

$$u_- = \frac{\beta}{1+2\alpha\beta} \quad \text{and} \quad u_+ = \frac{1+\beta}{1+2\alpha(1+\beta)}. \tag{S2}$$

In addition to these uniform steady states, nonuniform solutions may also exist, corresponding to polarized patterns on the sphere. Without loss of generality, the isotropy of the sphere allows us to define our η axis such that the cap is centered at $\eta = -1$ and $\bar{u}(\eta)$ is monotonically decreasing. For these cap-like profiles to exist, there must exist some regions where $\bar{u}(\eta) > \gamma$ and $\bar{u}(\eta) < \gamma$, respectively. Continuity and monotonicity of the profile therefore imply the existence of some $\eta = \eta_c \in (-1, 1)$ such that $\bar{u}(\eta_c) = \gamma$. The ODE may then be split into two distinct regions, corresponding to the presence or absence of autocatalytic recruitment:

$$0 = \delta^2 \frac{d}{d\eta}\left[(1-\eta^2)\frac{d\bar{u}}{d\eta}\right] + k\beta - \bar{u}, \qquad \eta > \eta_c, \tag{S3}$$

$$0 = \delta^2 \frac{d}{d\eta}\left[(1-\eta^2)\frac{d\bar{u}}{d\eta}\right] + k\,(\beta+1) - \bar{u}, \qquad \eta < \eta_c, \tag{S4}$$

where we introduced a constant

$$k := 1 - \alpha\int_{-1}^{1} \bar{u}\ \mathrm{d}\eta, \tag{S5}$$

that depends on the solution $\bar{u}(\eta)$.

We now solve the nonhomogeneous Equations (S3)-(S4). When $\eta > \eta_c$:

$$\frac{d}{d\eta}\left[(1-\eta^2)\frac{d\bar{u}}{d\eta}\right] - \frac{\bar{u}}{\delta^2} = -\frac{k\beta}{\delta^2}, \tag{S6}$$

whose particular solution is $u_p = k\beta$. The corresponding homogeneous ODE is of the form:

$$\frac{d}{d\eta}\left[(1-\eta^2)\frac{d\bar{u}}{d\eta}\right] + \mu(\mu+1)\bar{u} = 0, \qquad \mu := -\frac{1}{2} + \frac{1}{2}\sqrt{1-\frac{4}{\delta^2}}. \tag{S7}$$

One solution of this equation is given by $P_\mu(\eta)$, the Legendre function of the first kind, defined as

$$P_\mu(\eta) = {}_2F_1\left(-\mu, \mu+1; 1; \frac{1-\eta}{2}\right), \tag{S8}$$

where ${}_2F_1(a,b;c;z)$ is the hypergeometric function [1]. Explicitly, using the definition of μ (irrespectively of the choice of the analytic branch for $\delta < 2$) and the power series representation of the hypergeometric function we have

$$\begin{aligned} P_\mu(\eta) &= 1 + \sum_{n=1}^{\infty} \frac{(1-\eta)^n}{2^n (n!)^2} \prod_{l=0}^{n-1} (l-\mu)(l+1+\mu) \\ &= 1 + \sum_{n=1}^{\infty} \frac{(1-\eta)^n}{2^n (n!)^2} \prod_{l=0}^{n-1} \left(\frac{1}{\delta^2} + l + l^2\right), \end{aligned} \tag{S9}$$

where the series above converges absolutely for all $\eta \in (-1,1)$. Furthermore, by direct inspection of this formula we have $P_\mu(1) = 1$, $P_\mu(-1) = \infty$, and $P_\mu(\eta)$ is real-valued and strictly decreasing for all $\eta \in (-1,1)$. Therefore, in view of the reflection symmetry the second linearly independent solution of the above equation may be chosen to be $P_\mu(-\eta)$, and the general solution of Equation (S3) may be written as

$$\bar{u}(\eta > \eta_c) = c_1 P_\mu(\eta) + c_2 P_\mu(-\eta) + k\beta, \tag{S10}$$

for some constants $c_{1,2}$. Boundedness of the solution for $\eta > \eta_c$ implies that $c_2 = 0$ and monotonicity of the profile requires that $c_1 > 0$. In addition, for some $\eta_c \in (-1,1)$ we should have $\bar{u}(\eta_c) = \gamma$. This yields for $\gamma > \beta k$:

$$\bar{u}(\eta > \eta_c) = \frac{\gamma - \beta k}{P_\mu(\eta_c)} P_\mu(\eta) + k\beta. \tag{S11}$$

Equation (S4) may be solved in the same manner when $\eta < \eta_c$:

$$\frac{d}{d\eta}\left[(1-\eta^2)\frac{d\bar{u}}{d\eta}\right] - \frac{\bar{u}}{\delta^2} = -\frac{k(\beta+1)}{\delta^2}. \tag{S12}$$

A particular solution is $u_p = k(\beta+1)$, and the homogeneous equation is as before. Thus, the general solution is now:

$$\bar{u}(\eta < \eta_c) = c_3 P_\mu(-\eta) + c_4 P_\mu(\eta) + k(\beta+1), \tag{S13}$$

for some constants $c_{3,4}$. Boundedness and monotonicity imply $c_4 = 0$ and $c_3 < 0$, and the condition that $\bar{u}(\eta_c) = \gamma$ yields:

$$\bar{u}(\eta < \eta_c) = \frac{\gamma - (1+\beta)k}{P_\mu(-\eta_c)} P_\mu(-\eta) + k(1+\beta). \tag{S14}$$

Thus, we arrive at the nonuniform steady state solution in Equations (9)-(10) from the main text:

$$\bar{u}(\eta > \eta_c) = (\gamma - \beta k)\, \frac{P_\mu(\eta)}{P_\mu(\eta_c)} + \beta k, \tag{S15}$$

$$\bar{u}(\eta < \eta_c) = (\gamma - (1+\beta)k)\, \frac{P_\mu(-\eta)}{P_\mu(-\eta_c)} + (1+\beta)k. \tag{S16}$$

Smoothness at of the solution at $\eta = \eta_c$ requires matching first derivatives. Differentiating Equations (S15)-(S16) with respect to η and setting the two sides equal at $\eta = \eta_c$ yields an explicit equation for k in terms of model parameters that matches the relationship given in the main text:

$$k = \frac{\gamma \left(1 + \dfrac{P'_\mu(\eta_c)}{P'_\mu(-\eta_c)} \dfrac{P_\mu(-\eta_c)}{P_\mu(\eta_c)}\right)}{1 + \beta \left(1 + \dfrac{P'_\mu(\eta_c)}{P'_\mu(-\eta_c)} \dfrac{P_\mu(-\eta_c)}{P_\mu(\eta_c)}\right)}. \tag{S17}$$

Multiplying this expression through Equation (S16) allows $\bar{u}(\eta < \eta_c)$ to be written in a more convenient form that will allow for an expression for γ in terms of model parameters:

$$\bar{u}(\eta < \eta_c) = (\beta k - \gamma)\, \frac{P'_\mu(\eta_c)}{P'_\mu(-\eta_c)} \frac{P_\mu(-\eta)}{P_\mu(\eta_c)} + (1+\beta)k. \tag{S18}$$

Using Equation (S18) and the original definition of k defined for Equations (S3)-(S4) yields an integral equation that relates all model parameters:

$$\frac{\alpha\,(\gamma - \beta k)}{P_\mu(\eta_c)} \left[-\frac{P'_\mu(\eta_c)}{P'_\mu(-\eta_c)} \int_{-1}^{\eta_c} P_\mu(-\eta)\, \mathrm{d}\eta + \int_{\eta_c}^{1} P_\mu(\eta)\, \mathrm{d}\eta \right] + k(1 + \alpha(1+\eta_c) + 2\alpha\beta) = 1. \tag{S19}$$

Equations (S20)-(S23) highlight known properties of Legendre functions that allow for Equation (S19) to be simplified further:

$$\int_x^1 P_\mu(\eta)\, \mathrm{d}\eta = \frac{P_{\mu-1}(x) - P_{\mu+1}(x)}{2\mu+1}, \tag{S20}$$

$$P'_\mu(x) = \frac{\mu+1}{1-x^2} \left(x P_\mu(x) - P_{\mu+1}(x)\right), \tag{S21}$$

$$P'_\mu(-x) = -\frac{\mu+1}{1-x^2} \left(x P_\mu(-x) + P_{\mu+1}(-x)\right), \tag{S22}$$

$$(2\mu+1) x P_\mu(x) = \mu P_{\mu-1}(x) + (\mu+1) P_{\mu+1}(x). \tag{S23}$$

The integral expressions in Equation (S19) may be rearranged as

$$-\frac{P'_\mu(\eta_c)}{P'_\mu(-\eta_c)}\int_{-1}^{\eta_c} P_\mu(-\eta)\ \mathrm{d}\eta + \int_{\eta_c}^{1} P_\mu(\eta)\ \mathrm{d}\eta = -\frac{P'_\mu(\eta_c)}{P'_\mu(-\eta_c)}\int_{-\eta_c}^{1} P_\mu(y)\ \mathrm{d}y + \int_{\eta_c}^{1} P_\mu(\eta)\ \mathrm{d}\eta. \tag{S24}$$

Dividing all the terms in Equation (S23) by μ allows one to write $P_{\mu-1}(x)$ in terms of $P_\mu(x)$. This expression can be plugged into the definition of the integral in Equation (S20). The definitions of the derivatives given in Equations (S21)-(S22) yield the relationship given in Equation (S25):

$$-\frac{P'_\mu(\eta_c)}{P'_\mu(-\eta_c)}\int_{-\eta_c}^{1} P_\mu(y)\ \mathrm{d}y + \int_{\eta_c}^{1} P_\mu(\eta)\ \mathrm{d}\eta = 0. \tag{S25}$$

Substituting this result into Equation (S19) and using the expression for k given by Equation (S17) allows for γ to be expressed in terms of the model parameters, the key result of this analysis given as Equation (11) in the main text:

$$\gamma = \frac{1+\beta\left(1+\dfrac{P'_\mu(\eta_c)}{P'_\mu(-\eta_c)}\dfrac{P_\mu(-\eta_c)}{P_\mu(\eta_c)}\right)}{\left(1+\dfrac{P'_\mu(\eta_c)}{P'_\mu(-\eta_c)}\dfrac{P_\mu(-\eta_c)}{P_\mu(\eta_c)}\right)(1+\alpha(1+\eta_c)+2\alpha\beta)}. \tag{S26}$$

Existence and multiplicity of solutions of Equation (S1) is determined by the roots of the algebraic equation above and can be analyzed graphically for any specific set of the parameters $(\alpha, \beta, \gamma, \delta)$. As discussed in the main text, depending on the values of the parameters we generically find 1 or 3 distinct roots for Equation (S26), with the latter case observed for smaller values of δ. To see whether this situation persists, we carried out an asymptotic analysis of solutions of Equation (S26) for an important parameter regime of $\delta \ll 1$, in which the spherical cap profiles are characterized by sharp concentration gradients. In this case one can use WKB asymptotics of the Legendre functions (as obtained from Equation (S7)) to see that to the leading order

$$P_\mu(\eta)/P_\mu(0) \simeq (1-\eta^2)^{-1/4} e^{-\delta^{-1}\arcsin\eta}, \qquad \eta \in (-1,1), \tag{S27}$$

and, therefore, we have $P'_\mu(\eta)/P_\mu(\eta) \simeq -1/\left(\delta\sqrt{1-\eta^2}\right)$ for all $1-\eta^2 \gg \delta^2$ and $\delta \ll 1$. Substituting this expression into Equation (S26) yields for all $1-\eta_c^2 \gg \delta^2$ and all δ sufficiently small:

$$\gamma(\eta_c) \simeq \frac{2\beta+1}{2(1+\alpha(2\beta+1+\eta_c))}. \tag{S28}$$

A comparison between Equation (S26) and the scaling given by Equation (S28) in Figure S1 shows reasonable agreement when η_c is far away from the ends of the domain. In particular,

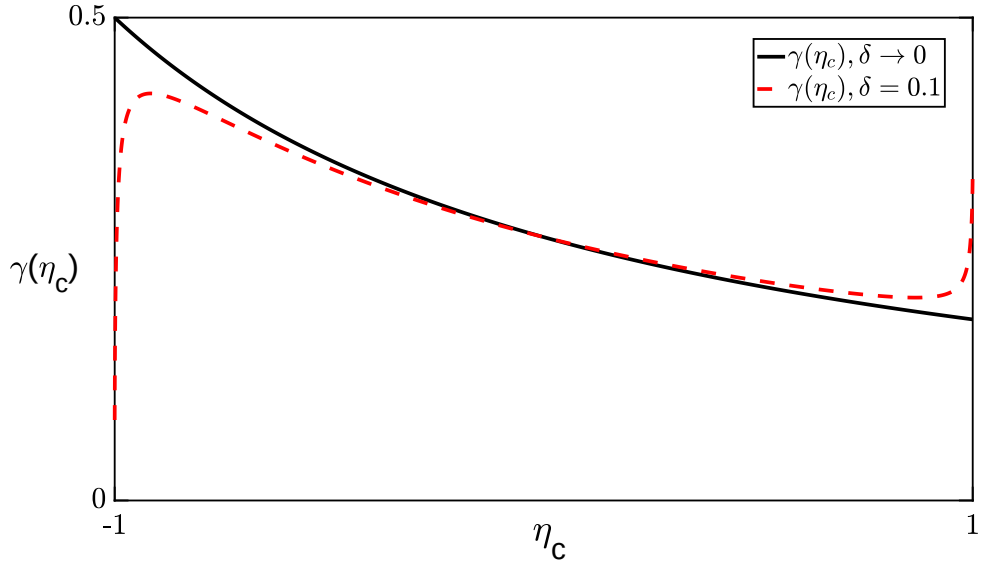

Figure S1: For $\alpha = 1, \beta = 0.1$, the curves defined by Equations S26 and S28 Here, it can be seen that this scaling is accurate for sufficiently small δ in the regime where $\gamma(\eta_c)$ in Equation S26 has a negative slope.

$\gamma(\eta_c)$ is a monotone decreasing function with $\gamma \in \left(\frac{2\beta+1}{2(1+2\alpha(\beta+1))}, \frac{2\beta+1}{2(1+2\alpha\beta)}\right)$. We refer to this branch of solutions as *large spherical caps*, in which the profile $\bar{u}(\eta)$ approaches a piecewise-constant function taking both values from Equation (S2). On the other hand, one can see from Equation (S9) that to the leading order in $\delta \ll 1$ we have

$$P_\mu(\eta) \simeq \sum_{n=0}^{\infty} \frac{(1-\eta)^n}{2^n \delta^{2n} (n!)^2} = I_0\left(\sqrt{2\delta^{-2}(1-\eta)}\right), \qquad 1-\eta = O(\delta^2), \tag{S29}$$

where $I_0(z)$ is the modified Bessel function of the first kind [1]. This formula can also be obtained by rewriting Equation (S7), using the variable $z = \arccos\eta$ and keeping only the leading order terms. Similarly, to the leading order in $\delta \ll 1$ we have

$$P_\mu(\eta) \sim K_0\left(\sqrt{2\delta^{-2}(1+\eta)}\right), \qquad 1+\eta = O(\delta^2), \tag{S30}$$

where $K_0(z)$ is the modified Bessel function of the second kind [1]. With this information at hand, we have for $\delta \ll 1$:

$$\frac{P'_\mu(\eta_c)}{P'_\mu(-\eta_c)} \frac{P_\mu(-\eta_c)}{P_\mu(\eta_c)} \simeq \frac{I_1\left(\sqrt{2\delta^{-2}(1-\eta_c)}\right) K_0\left(\sqrt{2\delta^{-2}(1-\eta_c)}\right)}{I_0\left(\sqrt{2\delta^{-2}(1-\eta_c)}\right) K_1\left(\sqrt{2\delta^{-2}(1-\eta_c)}\right)}, \qquad 1-\eta_c = O(\delta^2), \tag{S31}$$

which by inspection is a decreasing function of $\delta^{-2}(1-\eta_c)$ that approaches 0 as $\delta^{-2}(1-\eta_c) \to 0$, or 1 as $\delta^{-2}(1-\eta_c) \to \infty$. Thus, by Equation (S26) we have a unique solution for all γ

running through the interval $\gamma \in \left(\frac{2\beta+1}{2(1+2\alpha(\beta+1))}, \frac{\beta+1}{1+2\alpha(\beta+1)}\right)$, yielding what we call a *small spherical cap solution*, in which $\bar{u}(\eta)$ is close to the larger of the two values in Equation (S2) in most of the domain, with $1-\eta_c = O(\delta^2)$. Analogously, we alse have a small spherical cap solution for $\delta \ll 1$ and $\gamma \in \left(\frac{\beta}{1+2\alpha\beta}, \frac{2\beta+1}{2(1+2\alpha\beta)}\right)$, with $\bar{u}(\eta)$ taking mostly the smallest of the two values in Equation (S2) in most of the domain and with $1+\eta_c = O(\delta^2)$.

Linear Stability of Spherical Cap Solutions

We now perform a linear stability analysis of the spherical cap solutions. In our approach we follow [2], in which a very similar analysis of radial solutions in balls has been carried out in Sec. 13.2.2 (see also the original Refs. [3–5]).

We start by writing Equation (7), using (η, ϕ) as independent spatial variables:

$$\frac{\partial u}{\partial \tau} = -Lu - u + \left(1 - \frac{\alpha}{2\pi}\int_0^{2\pi}\int_{-1}^{1} u\, d\eta\, d\phi\right) g_\nu(u), \tag{S32}$$

where the operator L and the function g are defined as

$$L := -\delta^2 \frac{\partial}{\partial \eta}\left[(1-\eta^2)\frac{\partial}{\partial \eta}\right] - \frac{\delta^2}{1-\eta^2}\frac{\partial^2}{\partial \phi^2}, \qquad g_\nu(u) := \beta + \frac{u^\nu}{u^\nu + \gamma^\nu}, \tag{S33}$$

and linearize this equation around the steady state $\bar{u} = \bar{u}(\eta)$, which solves

$$0 = \delta^2 \frac{d}{d\eta}\left[(1-\eta^2)\frac{d\bar{u}}{d\eta}\right] - \bar{u} + k g_\nu(\bar{u}), \tag{S34}$$

where k was defined in Equation (S5). Fixing $m \in \mathbb{Z}$ and $\lambda_m \in \mathbb{R}$, substituting

$$u(\eta, \phi, \tau) = \bar{u}(\eta) + \varepsilon \psi_m(\eta) e^{im\phi - \lambda_m \tau} \tag{S35}$$

into Equation (S32) and sending $\varepsilon \to 0$, we arrive at the following equation for the eigenmodes ψ_m and their associated exponential decay/growth rates λ_m (depending on whether λ_m is positive/negative) at leading order in ε:

$$\lambda_m \psi_m = L_m \psi_m + \psi_m - k g_\nu'(\bar{u})\psi_m + \alpha g_\nu(\bar{u}) \int_{-1}^{1} \psi_m(\eta) d\eta, \qquad m = 0, \tag{S36}$$

$$\lambda_m \psi_m = L_m \psi_m + \psi_m - k g_\nu'(\bar{u})\psi_m, \qquad m \neq 0, \tag{S37}$$

where

$$L_m := -\delta^2 \frac{d}{d\eta}\left[(1-\eta^2)\frac{d}{d\eta}\right] + \frac{\delta^2 m^2}{1-\eta^2}, \qquad g'(\bar{u}) := \left.\frac{dg_\nu(u)}{du}\right|_{u=\bar{u}}, \tag{S38}$$

with natural boundary conditions $\psi_m(\eta) = O\left(|\eta \mp 1|^{\frac{|m|}{2}}\right)$ for $\eta \to \pm 1$. Note that in the limit $\nu \to \infty$ corresponding to the Heaviside function-type nonlinearity $g_\infty(u) = \lim_{\nu\to\infty} g_\nu(u) = \beta + H(u-\gamma)$ we recover

$$g_\infty'(\bar{u}(\eta)) = \delta(\eta - \eta_c)\left|\frac{d\bar{u}(\eta_c)}{d\eta}\right|^{-1}, \tag{S39}$$

where $\delta(z)$ is the one-dimensional Dirac delta-function.

Let us introduce the Sturm-Liouville operators H_m and their associated eigenpairs (ψ_m^n, λ_m^n), which satisfy

$$H_m\psi_m^n = \lambda_m^n\psi_m^n, \qquad H_m := L_m + 1 - kg'_\nu(\bar{u}), \qquad n = 0, 1, 2, \ldots. \tag{S40}$$

According to Sturm-Liouville theory, for each m all eigenvalues $\lambda_m^0 < \lambda_m^1 < \lambda_m^2 < \cdots \to \infty$ have multiplicity one, and each eigenvalue λ_m^n is associated to an eigenfunction with precisely n zeros in $(-1, 1)$. Furthermore, we have $\lambda_{m'}^0 > \lambda_m^0$ for all $|m'| > |m| \geq 0$. The latter can be easily seen from the fact that λ_m^0 minimizes the Rayleigh quotient associated with H_m:

$$R_m(\psi) := \frac{\int_{-1}^{1} \left\{\delta^2(1-\eta^2)|\psi'|^2 + \delta^2 m^2(1-\eta^2)^{-1}\psi^2 + \psi^2 - kg'_\nu(\bar{u})\psi^2\right\} d\eta}{\int_{-1}^{1} \psi^2 d\eta}. \tag{S41}$$

Therefore, we have

$$\lambda_m^0 = R_m(\psi_m^0) = \min_{\psi} R_m(\psi) \leq R_m(\psi_{m'}^0) < R_{m'}(\psi_{m'}^0) = \lambda_{m'}^0, \tag{S42}$$

where the minimization is carried out over all $\psi \in W_{loc}^{1,2}(-1, 1)$ satisfying $\int_{-1}^{1} \psi^2 d\eta = 1$.

We now observe that because of the rotational symmetry of the problem the operators $H_{\pm 1}$ have a zero eigenvalue associated with the eigenfunction

$$\psi_{\pm 1}^0(\eta) = \sqrt{1-\eta^2}\, \frac{d\bar{u}(\eta)}{d\eta}. \tag{S43}$$

Indeed, differentiating Equation (S34) with respect to η and multiplying the resulting equation by $\sqrt{1-\eta^2}$, after some algebra we obtain

$$\begin{aligned} 0 = -\delta^2\sqrt{1-\eta^2}\frac{d^2}{d\eta^2}\left[(1-\eta^2)\frac{d\bar{u}}{d\eta}\right] + (1 - kg'_\nu(\bar{u}))\sqrt{1-\eta^2}\,\frac{d\bar{u}}{d\eta} \\ = H_{\pm 1}\left[\sqrt{1-\eta^2}\,\frac{d\bar{u}}{d\eta}\right]. \end{aligned} \tag{S44}$$

Since for the spherical cap solutions the function $\bar{u}(\eta)$ is strictly monotone decreasing for all $\eta \in (-1, 1)$, we thus have that $\sqrt{1-\eta^2}\,\frac{d\bar{u}(\eta)}{d\eta}$ does not change sign and is, therefore, the eigenfunction associated with $\lambda_{\pm 1}^0 = 0$. This means, in particular, that

$$\lambda_m^n > 0 \qquad \forall m \neq 0 \text{ and } \forall n \geq 0 \qquad \text{or} \qquad \forall m = \pm 1 \text{ and } \forall n \geq 1. \tag{S45}$$

It is clear that for $m \neq 0$ the solutions of the obtained eigenvalue problem are the eigenpairs (ψ_m^n, λ_m^n) of the Sturm-Liouville operator H_m. Therefore, by Equation (S45) all the modes with $m \neq 0$ are linearly stable, except for the case $m = \pm 1$ and $n = 0$ corresponding to infinitesimal rotations, which are neutrally stable. Thus, stability of the spherical cap solutions is determined by the axially symmetric modes corresponding to $m = 0$.

Focusing now on the case $m = 0$, we first observe that in the absence of the nonlocal term in Equation (S32), i.e., when $\alpha = 0$, we must have $\lambda_0^0 < 0$, in view of Equation (S42)

and the fact that $\lambda_{\pm 1}^0 = 0$. Therefore, a sufficiently strong global feedback expressed by the integral term in Equation (S32) is required for the stability of spherical caps. To proceed with the analysis of (ψ_0, λ_0), which equivalently satisfy

$$H_0\psi_0 + \alpha g_\nu(\bar{u}) \int_{-1}^{1} \psi_0 \, d\eta = \lambda_0 \psi_0, \tag{S46}$$

we note that the operator in the left-hand side of Equation (S46) is the Sturm-Liouville operator H_0 plus a rank-one operator (generally, not self-adjoint). Therefore, if any of the eigenfunctions of H_0 satisfy $\int_{-1}^{1} \psi_0^n d\eta = 0$, then the pair (ψ_0^n, λ_0^n) is also a solution to Equation (S46). If not, then according to Fredholm alternative λ_0^n is still an eigenvalue of Equation (S46), if $\int_{-1}^{1} g_\nu(\bar{u})\psi_0^n d\eta = 0$.

On the other hand, for all $\lambda_0 \neq \lambda_0^n$ we can rewrite Equation (S46) as (see also [6])

$$\psi_0 = -\alpha (H_0 - \lambda_0)^{-1} g_\nu(\bar{u}) \int_{-1}^{1} \psi_0 \, d\eta, \tag{S47}$$

and integrating the resulting expression yields

$$1 + \alpha \int_{-1}^{1} (H_0 - \lambda_0)^{-1} g_\nu(\bar{u}) \, d\eta = 0. \tag{S48}$$

We now investigate under which conditions one may have $\lambda_0 < 0$, signifying linear instability of the spherical cap solutions. Observe first that λ_0 cannot equal λ_0^0, as ψ_0^0 corresponds to the ground state of R_0 and, therefore, has constant sign. On the other hand, for large enough n we have $\lambda_0^n > 0$, so in order to verify whether the condition

$$\lambda_0^n < 0 \qquad \text{and} \qquad \int_{-1}^{1} \psi_0^n d\eta = 0 \text{ or } \int_{-1}^{1} g_\nu(\bar{u})\psi_0^n d\eta = 0, \tag{S49}$$

is satisfied for some $n \geq 1$, one only needs to verify Equation (S49) for finitely many $n \geq 1$, if any.

If $\lambda_0 \neq \lambda_0^n$ for all $n \geq 0$, then Equation (S48) must be satisfied. To analyze its solutions, we expand its right-hand side with respect to the complete orthogonal basis of the eigenfunctions ψ_0^n of H_0:

$$1 + \alpha \sum_{n=0}^{\infty} \frac{a_n}{\lambda_0^n - \lambda_0} = 0, \qquad a_n := \frac{\int_{-1}^{1} \psi_0^n d\eta \int_{-1}^{1} g_\nu(\bar{u})\psi_0^n d\eta}{\int_{-1}^{1} |\psi_0^n|^2 d\eta}. \tag{S50}$$

Recall that in this formula $\lambda_0^0 < 0$, and we also have $a_0 > 0$, since ψ_0^0 has a constant sign.

For $\omega \in \mathbb{C}$, defining

$$D(\omega) := 1 + \alpha \sum_{n=0}^{\infty} \frac{a_n}{\lambda_0^n + i\omega}, \tag{S51}$$

we observe that the zeros of $D(\omega)$ with $\omega = i\lambda_0$ in the lower half-plane of the complex frequency ω would correspond to linearly unstable modes. It is convenient to study the

number of zeros of $D(\omega)$ in the lower-half plane, using the Cauchy argument principle, which states that the number of zeros of this function is equal to

$$N = P + \frac{1}{2\pi}\Delta \arg D(\omega), \tag{S52}$$

where P is the number of poles there and $\Delta \arg D(\omega)$ is the change of the argument of the function $D(\omega)$ as ω runs from $+\infty$ to $-\infty$ along the real axis. Thus, the number of negative eigenvalues of H_0 and the winding number of $\arg D(\omega)$ ultimately encode the stability of the solution.

The analysis of Equation (S52) requires the precise information on the spectrum of H_0 and the magnitudes of a_n (for an example of an analytical treatment in a related context, see [7]). For $\nu = \infty$ this problem may once again be treated with the help of the Legendre functions, similarly to the way we constructed the spherical cap solutions. It is not diffucult to see that in this case the eigenfunctions of H_0 normalized to equal 1 at $\eta = \eta_c$ must satisfy

$$\psi_0^n(\eta) = \begin{cases} \frac{P_{\mu_0^n}(-\eta)}{P_{\mu_0^n}(-\eta_c)} & -1 < \eta < \eta_c, \\ \frac{P_{\mu_0^n}(\eta)}{P_{\mu_0^n}(\eta_c)} & \eta_c < \eta < 1, \end{cases} \qquad \mu_0^n := -\frac{1}{2} + \frac{1}{2}\sqrt{1 - \frac{4(1-\lambda_0^n)}{\delta^2}}, \tag{S53}$$

assuming $P_{\mu_0^n}(\pm\eta_c) \neq 0$. In turn, the eigenvalues λ_0^n are obtained from the solution of the algebraic equation

$$\frac{\delta^2(1-\eta_c^2)}{k}\left|\frac{d\bar{u}(\eta_c)}{d\eta}\right|\left(\frac{P'_{\mu_0^n}(\eta_c)}{P_{\mu_0^n}(\eta_c)} + \frac{P'_{\mu_0^n}(-\eta_c)}{P_{\mu_0^n}(-\eta_c)}\right) = -1, \tag{S54}$$

where k is defined in Equation (S17) and $\frac{d\bar{u}(\eta_c)}{d\eta}$ is obtained by differentiating $\bar{u}(\eta)$ from Equation (S15) and setting $\eta = \eta_c$. Equation (S54) is obtained by matching the jump of the derivative of $\psi_0^n(\eta)$ at $\eta = \eta_c$ due to the delta-function in the definition of H_0.

To get some physical insight into instability we may observe that the coefficients a_n in Equation (S50) are expected to be rapidly decreasing with n, while λ_0^n are, in turn, rapidly increasing in n. Therefore, it may not be unreasonable to approximate the function $D(\omega)$ by keeping only the first term in the series [2]. We would then arrive at the expression

$$D(\omega) \approx 1 - \frac{\alpha a_0}{|\lambda_0^0| - i\omega}, \tag{S55}$$

where we explicitly took into account that $\lambda_0^0 < 0$. For this choice of $D(\omega)$ we can conclude that $P = 1$ and the image of $D(\omega)$ is a simple closed contour oriented clockwise. Thus, whether $D(\omega)$ has a zero in the lower half-plane depends on whether or not this contour encloses the origin. Checking the sign of $D(0)$, we then arrive at an approximate instability criterion:

$$\alpha \lesssim \frac{|\lambda_0^0|}{a_0}. \tag{S56}$$

As expected, all spherical cap solutions should be unstable for all sufficiently small α, while stability may be achieved for sufficiently large values of α. For a representative set of parameters $(\alpha, \beta, \gamma, \delta) = (1, 0, 0.28, 0.4)$ corresponding to a large spherical cap, solving Equation (S54) numerically yields $\{\lambda_0^n\}_{n=0}^4 = \{-0.216,\ 1.228,\ 1.798,\ 2.513,\ 4.187\}$, and corresponding $\{a_n\}_{n=0}^4 = \{0.545,\ -0.142,\ 0.195,\ 0.010,\ -0.005\}$. Keeping only λ_0^0 and a_0, we get the bound for instability $\alpha < 0.396$, while the bound for instability from using these first five terms gives $\alpha < 0.395$, in excellent agreement with the heuristics provided before Equation (S56). In particular, the solution for these values of the parameters is linearly stable.

One can give a more precise argument for stability of large spherical caps (i.e., those for which the value of $\eta = \eta_c$ at which the threshold $\gamma = \bar{u}(\eta_c)$ is reached, see Equation (S26), is not too close to $\eta = \pm 1$) in the case $\nu = \infty$ and $\delta \ll 1$. First of all, in the case of the Heaviside nonlinearity the operator H_0 has exactly one negative eigenvalue. In fact, it is not difficult to see that all $\lambda_0^n > 1$ for $n \geq 1$ in this case. Indeed, introduce a change of variables

$$\eta = \tanh z, \qquad z \in (-\infty, +\infty). \tag{S57}$$

Then the equation for the eigenfunctions of H_0 becomes (with a slight abuse of notation, using the same letters to denote the corresponding functions of z)

$$-\delta^2 \frac{d^2\psi_0^n}{dz^2} + \cosh^{-2} z \left(1 - k \left|\frac{d\bar{u}(z_c)}{dz}\right|^{-1} \delta(z - z_c)\right) \psi_0^n = \lambda_0^n \psi_0^n \cosh^{-2} z, \tag{S58}$$

where $z_c \in \mathbb{R}$ is such that $\eta_c = \tanh z_c$.

Consider now $\psi_0^n(z)$ with $n \geq 1$, and without loss of generality assume that $\psi_0^n(z_0) = 0$ for some $z_0 \geq z_c$, and that $d\psi_0^n(z_0)/dz > 0$. Then if $\lambda_0^n \leq 1$, the function ψ_0^n satisfies

$$\frac{d^2\psi_0^n(z)}{dz^2} = (1 - \lambda_0^n)\delta^{-2}\psi_0^n(z) \cosh^{-2} z \geq 0 \qquad \forall z \in (z_0, +\infty). \tag{S59}$$

Thus, $\psi_0^n(z) \geq C(z - z_0)$ for some $C > 0$ and, therefore, we have $\psi_0^n(z) \to \infty$ as $z \to +\infty$, contradicting boundedness of the eigenfunctions of H_0 for any $n \geq 1$.

We thus established that for $\nu = \infty$ we have $P = 1$ in Equation (S52). Next we note that for $\delta \ll 1$ the eigenvalues of H_0 behave as $\lambda_0^n - 1 \sim n^2\delta^2$ for $n \geq 1$. This allows us to use a local approximation

$$\sum_{n=1}^{\infty} \frac{a_n}{\lambda_0^n + i\omega} \simeq \frac{a_\infty - a_0}{1 + i\omega}, \qquad a_\infty := \int_{-1}^{1} g_\infty(\bar{u})\, d\eta, \tag{S60}$$

in the case $\delta \ll 1$, which is obtained by replacing λ_0^n in Equation (S50) with 1 and using completeness of the family $(\psi_0^n)_{n=0}^\infty$. Putting everything together yields

$$D(\omega) \simeq 1 - \alpha \left(\frac{a_0}{|\lambda_0^0| - i\omega} + \frac{a_0}{1 + i\omega} - \frac{a_\infty}{1 + i\omega}\right). \tag{S61}$$

To conclude, we observe that as $\delta \to 0$ we have

$$a_0 = O(\delta) \qquad \text{and} \qquad \lambda_0^0 = O(\delta^2). \tag{S62}$$

To see this, write the equation for $\bar{u} = \bar{u}(z)$:

$$0 = \delta^2 \frac{d^2\bar{u}}{dz^2} - (\bar{u} - k g_\infty(\bar{u})) \cosh^{-2} z, \qquad g_\infty(\bar{u}(z)) = \beta + H(z_c - z). \tag{S63}$$

Solving Equation (S63) to the leading order in $\delta \ll 1$, we obtain

$$\bar{u}(z) \simeq \begin{cases} k\beta + \frac{1}{2} k e^{-\frac{z - z_c}{\delta \cosh z_c}}, & z \geq z_c, \\ k(\beta + 1) - \frac{1}{2} k e^{-\frac{z_c - z}{\delta \cosh z_c}}, & z < z_c. \end{cases} \tag{S64}$$

In particular, we have

$$\frac{d\bar{u}(z)}{dz} \simeq -\frac{k}{2\delta \cosh z_c} e^{-\frac{|z - z_c|}{\delta \cosh z_c}}. \tag{S65}$$

Similarly, Equation (S58) with $n = 0$ is

$$-\delta^2 \frac{d^2\psi_0^0}{dz^2} + \cosh^{-2} z \left(1 - k \left| \frac{d\bar{u}(z_c)}{dz} \right|^{-1} \delta(z - z_c)\right) \psi_0^0 = \lambda_0^0 \psi_0^0 \cosh^{-2} z, \tag{S66}$$

and its solution to the leading order in $\delta \ll 1$, corresponding to $\lambda_0^0 \simeq 0$ to $O(\delta)$, is explicitly

$$\psi_0^0(z) \simeq \frac{d\bar{u}(z)}{dz}, \tag{S67}$$

noting that $d\bar{u}(z)/dz$ from Equation (S65) does not change sign. Substituting this expression, after a suitable normalization, into the definition of a_0 in Equation (S50), we obtain, again to the leading order in $\delta \ll 1$:

$$a_0 \simeq 2\delta(2\beta + 1)\sqrt{1 - \eta_c^2}, \tag{S68}$$

where we took into account that $\cosh^{-2} z_c = 1 - \eta_c^2$.

At the same time, by Equation (S44) we have

$$-\delta^2 \frac{d^2\psi_{\pm 1}^0}{dz^2} + \delta^2 \psi_{\pm 1}^0 + \cosh^{-2} z \left(1 - k \left| \frac{d\bar{u}(z_c)}{dz} \right|^{-1} \delta(z - z_c)\right) \psi_{\pm 1}^0 = 0. \tag{S69}$$

Therefore, to the leading order in $\delta \ll 1$ we obtain from Equation (S43):

$$\psi_{\pm 1}^0(z) \simeq \cosh^{-1} z_c \frac{d\bar{u}(z)}{dz}. \tag{S70}$$

We now multiply Equation (S69) by ψ_0^0 and integrate over the real line. Likewise, we multiply Equation (S66) by $\psi_{\pm 1}^0$ and integrate. Subtracting the obtained results yields

$$\delta^2 \int_{-\infty}^{\infty} \psi_0^0 \psi_{\pm 1}^0 dz = -\lambda_0^0 \int_{-\infty}^{\infty} \psi_0^0 \psi_{\pm 1}^0 \cosh^{-2} z \, dz. \tag{S71}$$

Thus, to the leading order in $\delta \ll 1$ we have, with the help of Equation (S67) and Equation (S70):

$$\lambda_0^0 \simeq -\frac{\delta^2}{1-\eta_c^2}, \tag{S72}$$

where we again used the fact that $\cosh^{-2} z_c = 1 - \eta_c^2$.

Finally, since by the definition in Equation (S60) we have

$$a_\infty = 2\beta + \eta_c + 1, \tag{S73}$$

and, hence, $a_\infty = O(1)$ as $\delta \to 0$, we may conclude by inspection of

$$D(\omega) \simeq 1 - \frac{\alpha a_0 |\lambda_0^0|}{|\lambda_0^0|^2 + \omega^2} + \frac{\alpha(a_\infty - a_0)}{1+\omega^2} - i\alpha\omega\left(\frac{a_0}{|\lambda_0^0|^2+\omega^2} + \frac{a_\infty - a_0}{1+\omega^2}\right), \tag{S74}$$

that $\omega \operatorname{Im} D(\omega) < 0$ and $D(0) < 0$ for all $\delta \ll 1$ and $\eta_c \in (-1, 1)$ fixed. Therefore, in this case $\Delta \arg D(\omega) = -2\pi$, and by Equation (S52) there are no negative eigenvalues for large spherical caps in the limit $\delta \to 0$. In other words, large spherical caps are always linearly stable for $\delta \ll 1$, $1 - \eta_c^2 = O(1)$ and $\alpha = O(1)$. More precisely, for $\delta \ll 1$ and η_c not approaching ± 1 a spherical cap solution is linearly stable if and only if

$$\alpha > \alpha_c, \qquad \alpha_c \simeq \frac{\delta}{2(2\beta+1)(1-\eta_c^2)^{3/2}}. \tag{S75}$$

where the asymptotic value of α_c is obtained by setting $D(0) = 0$, to the leading order in $\delta \ll 1$, and using the asymptotic expressions in Equation (S68) and Equation (S72). The instability is a consequence of Equation (S52) and the fact that $\Delta \arg D(\omega) = 0$ when $D(0) > 0$. Notice that by Equation (S28) at $\alpha = O(\delta)$ the large cap solution exists only in a narrow range of values of γ of width $O(\delta)$. At the same time, when $\alpha \gg 1$, the range of γ for existence narrows again to $O(\alpha^{-1})$, unless $\beta \lesssim \alpha^{-1}$. Lastly, it is easy to see that for small cap solutions one should expect $|\lambda_0^0| = O(1)$ and $a_0 = O(\delta^2)$, since for those solutions $\bar{u}(\eta)$ is close to constant, unless $1 - \eta^2 = O(\delta^2)$. Therefore, by the previous arguments the small spherical cap solutions are always unstable for $\delta \ll 1$.

Estimating Spatial Variation of Cytoplasmic Component

We now examine under which conditions the approximation of constant concentration of the species on the cell membrane used to derive Equation (7) in the main body of the paper is reasonable. To this end, we estimate the relative deviation of the concentration C on $\partial\Omega$ from its average $\bar{C}$ by solving Equations (1)–(3) at steady state with a prescribed steady state profile of the membrane bound species B. Notice that since C solves the Laplace's equation in Ω, we have that $\bar{C}$ is also the average value of C in Ω.

We expand the solution $C = C(\rho, \theta, \phi)$ of Equation (1) written in spherical coordinates, using spherical harmonics Y_l^m in Ω:

$$C(\rho, \theta, \phi) = \sum_{l=0}^{\infty} \sum_{m=-l}^{l} C_l^m (\rho/r)^l Y_l^m(\theta, \phi). \tag{S76}$$

From this formula, we have that the normal flux appearing in the left-hand side of Equation (3), as well as the solution itself on $\partial\Omega$ may be written as

$$D_C(n\cdot\nabla C)|_{\partial\Omega}=D_C\sum_{l=0}^{\infty}\sum_{m=-l}^{l}lr^{-1}C_l^mY_l^m(\theta,\phi),\qquad C|_{\partial\Omega}=\sum_{l=0}^{\infty}\sum_{m=-l}^{l}C_l^mY_l^m(\theta,\phi).\quad\text{(S77)}$$

On the other hand, we can also write the following expansions for B and $-\Delta_{\partial\Omega}B$ on $\partial\Omega$:

$$B(\theta,\phi)=\sum_{l=0}^{\infty}\sum_{m=-l}^{l}B_l^mY_l^m(\theta,\phi),\qquad -\Delta_{\partial\Omega}B(\theta,\phi)=\sum_{l=0}^{\infty}\sum_{m=-l}^{l}l(l+1)r^{-2}B_l^mY_l^m(\theta,\phi).\quad\text{(S78)}$$

Noting that by Equations (1) and (3) at steady state we have $D_C(n\cdot\nabla C)|_{\partial\Omega}=D_B\Delta_{\partial\Omega}B$, from the above two equations we can see that for all $l\neq 0$ we have

$$D_CC_l^m=-D_B(l+1)r^{-1}B_l^m,\quad\text{(S79)}$$

and, therefore, there holds

$$D_C^2\sum_{l=1}^{\infty}\sum_{m=-l}^{l}|C_l^m|^2=\frac{D_B^2}{r^2}\sum_{l=1}^{\infty}\sum_{m=-l}^{l}(l+1)^2|B_l^m|^2\leq\frac{2D_B^2}{r^2}\sum_{l=1}^{\infty}\sum_{m=-l}^{l}l(l+1)|B_l^m|^2.\quad\text{(S80)}$$

Thus, from Parseval's identity and integration by parts we obtain

$$\begin{aligned}D_C^2\int_0^{2\pi}\int_0^{\pi}|C(r,\theta,\phi)-\bar{C}|^2\sin\theta\,d\theta\,d\phi&\leq-\frac{2D_B^2}{r^2}\int_0^{2\pi}\int_0^{\pi}B(\theta,\phi)\Delta_{\mathbb{S}^2}B(\theta,\phi)\sin\theta\,d\theta\,d\phi\\&=\frac{2D_B^2}{r^2}\int_0^{2\pi}\int_0^{\pi}|\nabla_{\mathbb{S}^2}B(\theta,\phi)|^2\sin\theta\,d\theta\,d\phi.\end{aligned}\quad\text{(S81)}$$

Thus, we have found that on average the relative deviation of the concentration C on the cell membrane from its average value $\bar{C}$ in the cytosol is

$$\sqrt{\left\langle\left(\frac{C-\bar{C}}{\bar{C}}\right)^2\right\rangle_{\partial\Omega}}=\sqrt{\int_{\partial\Omega}\frac{|C-\bar{C}|^2}{4\pi r^2\bar{C}^2}dA}\leq\frac{D_B\max B}{D_C\bar{C}r}\sqrt{\frac{1}{2\pi\max B^2}\int_{\partial\Omega}|\nabla B|^2dA}.\quad\text{(S82)}$$

Notice that apart from the expression inside the square root in the right-hand side of Equation (S82), which is scale-free and thus only weakly depends on the solution for B (for example, this expression is bounded by $1/4$ when B is an exponentially decaying profile as a function of θ), the left-hand side of Equation (S82) is controlled by

$$\sqrt{\left\langle\left(\frac{C-\bar{C}}{\bar{C}}\right)^2\right\rangle_{\partial\Omega}}\leq\frac{MD_BN_B}{3D_CN_C},\quad\text{(S83)}$$

where $N_B = 4\pi r^2 \max B$ is the maximum number of molecules that can be bound to the cell membrane, $N_C = \frac{4}{3}\pi r^3 \bar{C}$ is the number of molecules in the cytosol, and M is the solution profile shape factor given by the square root in the right-hand side of Equation (S82) and expected to be of order unity. Thus, neglecting the variations of C across the cell membrane is justified whenever the surface diffusion is much slower than the bulk diffusion, as well as when the number of membrane bound molecules is smaller than that in the bulk. Using [8], we have $D_B = 0.03\ \mu\text{m}^2\ \text{s}^{-1}$, $D_C = 11\ \mu\text{m}^2\ \text{s}^{-1}$, $k_b = 0.28\ \mu\text{m}\ \text{s}^{-1}$, $k_d = 1\ \text{s}^{-1}, C_0 = 11.621\ \mu\text{m}^{-3}$, and $r = 3.95\ \mu$m. An appropriate choice of Γ to produce a spherical cap gives $N_B = 643$, $N_C = 2749$, and $M = 1.523$, which gives an upper bound of 3.24×10^{-4} for the left-hand side in Equation (S83), which is clearly negligible. Of course, in reality the estimate in (S83) is fairly conservative, and so in practice neglecting the variations of C should always provide a very good approximation.

Parametric Analysis of Localized Patterns

Recall the five dimensionless groups defined in Equation (7) of the main text:

$$\alpha := \frac{3}{2}\frac{k_b}{k_d r}, \quad \gamma := \frac{k_d \Gamma}{k_b C_0}, \quad \delta := \frac{1}{r}\sqrt{\frac{D_B}{k_d}}, \quad \nu, \text{ and } \beta.$$

Here, we analyze how perturbations with respect to various biological and kinetic parameters affect the formation of the stable spherical cap. Because β has no functional dependence on any other biological parameters within the system, we shall only consider the relationships between α, γ, and δ for $\nu \to \infty$ in this section.

In this regime, we have demonstrated that the four remaining dimensionless groups satisfy Equation (11) of the main text when a stable spherical cap may be formed. Thus, by fixing one of α, γ, or δ and keeping β constant, we may draw two-dimensional curves that define the edge of stability for spherical cap solutions, as shown in Figure S2. Using the definitions of these dimensionless groups, we may observe the effects of varying different constants.

The biological parameters Γ and C_0 only appear as terms in the definition of γ. Therefore, perturbing these cellular properties has the effect of changing γ only, with no effect on α or δ. As can be seen in Figure $3B$ of the main text, for a large enough perturbation of γ in either direction, a system that initial allows for polarization may leave the domain of stability and eventually only yield a homogeneous steady state. In a similar way, D_B only affects δ, but it can be seen that only a sufficient increase in D_B may cause stable steady state solutions to become unstable.

As both α and δ are proportional to $1/r$, increasing and decreasing the radius can induce instability for cap-like solutions, as shown in Figure S2. Because the effect on γ of decreasing k_b is the inverse of its effect on α, Figure S2 highlights that polarization will eventually disappear. However, increasing k_b appears to only have this effect for polarizable systems with small α and large γ; outside this regime, the system remains stable as it approaches an asymptote along the edge of stability. A similar effect can be seen by changing k_d. However, in this case, all dimensionless groups are affected by its variation.

Analytical Computations

Given a set of parameters $(\alpha, \beta, \gamma, \delta)$, $u(\eta)$, the axisymmetric steady state spherical cap

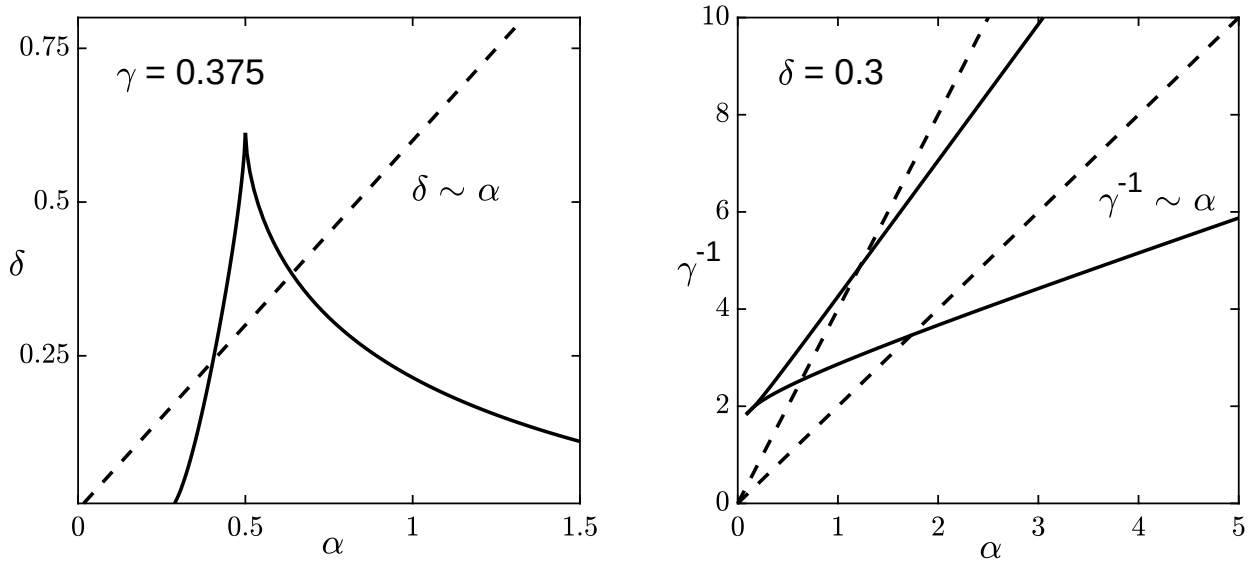

Figure S2: Left: *Bifurcation diagram of δ vs. α for $\beta = 0.1, \gamma = 0.375$. The dashed line represents the change in α and δ as cell radius is varied. For the symmetry breaking quadruple $(\alpha, \beta, \gamma, \delta) = (0.5, 0.1, 0.375, 0.3)$, both increasing or decreasing the cell radius eventually results in a loss of stable cap solution.* Right: *Bifurcation diagram of γ^{-1} vs. α for $\beta = 0.1, \delta = 0.3$. Here, the dashed lines highlight the dependence of α and γ with respect to the binding rate constant k_b.*

profile originating from $\eta = -1$, may be plotted by using Equations (9)-(10) of the main text. Here, the `LegendreP[,]` function in Mathematica is used to calculate both $u(\eta)$ and the $\gamma(\eta_c)$ profile described by Equation 11 of the main text.

Equation (11) defines a region in the parameter space of $(\alpha, \beta, \gamma, \delta)$ where spherical cap solutions are stable steady states. Here, one may plot γ as a function of α, β, and δ for $\eta_c \in (-1, 1)$ to observe its behavior. For sufficiently large δ at a given α and β, this function becomes monotonically increasing in the domain of η_c. For some fixed value of $\gamma = \gamma^*$, the equation $\gamma(\eta_c) - \gamma^* = 0$ will have only one root, corresponding to one value of η_c that gives a symmetry broken solution under this parameter set. This solution must be unstable by the heuristic identified in the main text; if γ^* is increased under these conditions, the profile would suggest a larger value of η_c satisfies the root of the equation, corresponding to a larger cap. If γ is the threshold by which patterns may form, increasing the value for γ should intuitively decrease the possible cap size, implying the original solution corresponded to an unstable pattern. Thus, stable patterns are restricted to locally decreasing regions of $\gamma(\eta_c)$ in the domain $\eta_c \in (-1, 1)$.

As δ decreases, the γ profile becomes N-shaped, suggesting the existence of a critical value of δ where $\gamma(\eta_c)$ loses its monotonicity, with some $\eta_c < 0$ yielding a local maximum for $\gamma(\eta_c)$ and some $\eta_c > 0$ yielding a local minimum. For a given set of (α, β, δ) where $\gamma(\eta_c)$ exhibits cubic-like behavior, the `D[,]` and `FindRoot[]` functions in Mathematica allow for the value of η_c to be found that correspond to the maximum and minimum. Direct calculation of γ for each δ at these points form the edge of stability for spherical caps at fixed α

and β. Connecting these points creates a cusp-like region in parameter space, as shown in Figure 3*B* of the main text. This process bounds the region where stable spherical caps may form, and for a set of parameters $(\alpha, \beta, \gamma, \delta)$, one can identify whether polarization is possible.

Numerical Analysis with Chebfun

The PDE from Equation (7) in the main text is a standard semi-linear PDE of the form

$$\frac{\partial u}{\partial \tau} = \delta^2 \nabla^2_{\mathbb{S}^2} u + \mathcal{N}(u), \tag{S84}$$

with the nonlinear operator $\mathcal{N}(u)$ given by:

$$\mathcal{N}(u) = \left(1 - \frac{\alpha}{2\pi} \int_0^{2\pi} \int_0^{\pi} u \sin\theta \, \mathrm{d}\theta \, \mathrm{d}\phi\right) (\beta + H(u - \gamma)) - u. \tag{S85}$$

To solve PDEs of this form, the Double Fourier Sphere (DFS) method is used in space [9] and an implicit-explicit algorithm is used in time. The DFS method is based on two-dimensional (2D) truncated Fourier series,

$$u(t, \phi, \theta) \approx \sum_{j=-m/2}^{m/2\,\prime} \sum_{k=-n/2}^{n/2\,\prime} \hat{u}_{jk}(t) \exp(i(j\theta + k\phi)), \tag{S86}$$

on an equidistant $n \times m$ longitude-latitude grid, where the primes on the summation signs indicate that the boundary terms $j = \pm m/2$ and $k = \pm n/2$ are halved. When Equation (S86) is substituted into the general semi-linear form of the PDE, a system of nm ODEs for the Fourier coefficients $\hat{u}_{jk}(t)$ given by $\hat{u}' = \delta^2 \mathbf{L}\hat{u} + \mathbf{N}(\hat{u})$ is obtained, where $\mathbf{L}$ (a $nm \times nm$ matrix) and $\mathbf{N}$ are the discretized versions of $\nabla^2_{\mathbb{S}^2}$ and $\mathcal{N}$, respectively. $\mathbf{L}$ is a block-diagonal matrix with banded blocks and may be inverted in $\mathcal{O}(mn)$ operations. The nonlinear operator $\mathbf{N}$ can be decomposed as $\mathbf{N}(\hat{u}) = \mathbf{N}_1(\hat{u})\mathbf{N}_2(\hat{u}) - \hat{u}$, where $\mathbf{N}_1$ and $\mathbf{N}_2$ are given by:

$$\mathbf{N}_1(\hat{u}) = 1 - \frac{\alpha}{2\pi} \int_0^{2\pi} \int_0^{\pi} u \sin\theta \, \mathrm{d}\theta \, \mathrm{d}\phi \approx 1 - \alpha \sum_{j=-m/2}^{m/2-1} \hat{u}_{j0}(t) \frac{1 + \exp(ij\pi)}{1 - j^2}, \tag{S87}$$

$$\mathbf{N}_2(\hat{u}) = \mathbf{F}(\beta + H(\mathbf{F}^{-1}\hat{u} - \gamma)), \tag{S88}$$

where $\mathbf{F}$ denotes the 2D fast Fourier transform (FFT). Here, the standard implicit-explicit IMEX-BDF4 scheme is used for time-stepping:

$$\begin{aligned}(25\mathbf{I}_{nm} - 12h\mathbf{L})\hat{u}^{n+1} = {} & 48\hat{u}^n - 36\hat{u}^{n-1} + 16\hat{u}^{n-2} - 3\hat{u}^{n-3} \\ & + 48h\mathbf{N}(\hat{u}^n) - 72h\mathbf{N}(\hat{u}^{n-1}) + 48h\mathbf{N}(\hat{u}^{n-2}) - 12h\mathbf{N}(\hat{u}^{n-3}),\end{aligned} \tag{S89}$$

with time-step h and $\hat{u}^n = \hat{u}(t_n)$. At each time-step, a linear system is solved to obtain the Fourier coefficients $\hat{u}^{n+1}$ at linear cost. Therefore, the dominant cost in Equation (S89) is the $\mathcal{O}(mn \log mn)$ 2D FFT for the nonlinear evaluations. Because this is a multi-step formula, it must be started with a one-step scheme. In this case, we use the LIRK4 algorithm.

As a test case, we solved the problem with the following parameters: $\alpha = 1$, $\beta = 0.1$,

$\gamma = 0.3$ and $\delta^2 = 0.05$, with the initial condition $u(t = 0, x, y, z) = \exp(-2(x^2+y^2+(z-1)^2)$, up to $\tau = 50$. Here, we used the time-step $h = 0.1$ over various grid sizes $m = n$, with a smooth approximation of the Heaviside function, $H(x) \approx (1 + \exp(-2\mu x))^{-1}$ where $\mu = m/(5 \log m)$. The exact solution at steady state was found analytically through substitution into Equations (9)-(10) of the main text. We then computed the relative L^2-error between exact and computed solutions as a function of the number of grid points. In this case, we obtained a nearly quadratic convergence in space (see Figure S3).

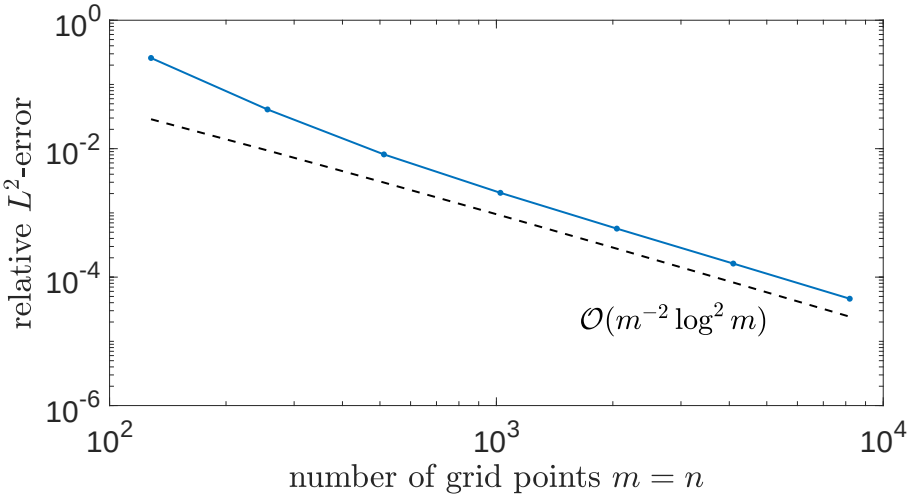

Figure S3: *Relative L^2-error between exact and computed solutions. The convergence is quadratic in space (up to logarithmic factors).*

Following [10], independent, normally distributed initial conditions are obtained by truncated spherical harmonic expansions with normalized, random coefficients $c_{\ell,j} \sim \mathcal{N}(0, 1)$, given by:

$$u(t = 0, \phi, \theta) = \sum_{\ell=0}^{m} \sum_{j=-\ell}^{\ell} c_{\ell,j} Y_{\ell,j}(\phi, \theta) = \sum_{\ell=0}^{m} \sum_{j=-\ell}^{\ell} c_{\ell,j} P_\ell^j(\cos\theta) \exp(ij\phi), \tag{S90}$$

for $Y_{\ell,j}$, the spherical harmonic of degree ℓ and order j and P_ℓ^j, the (normalized) associated Legendre polynomial. Functions of maximum wavelength, λ, are obtained for $m = 2\pi/\lambda$. All values for $u(t = 0, \phi, \theta)$ are then scaled appropriately so they are non-negative have a mean less than $1/(2\alpha)$.

Localization of Spherical Cap by Convection

The effect of cortical flows was modeled by adding a new term to the equation for the membrane species:

$$\frac{\partial B}{\partial t} = D_B \nabla^2_{r\mathbb{S}^2} B - \nabla \cdot (\mathbf{v}B) + k_b \left(\beta + \frac{B^\nu}{B^\nu + \Gamma^\nu}\right) C - k_d B, \tag{S91}$$

where $\mathbf{v} = (\mathbf{v}_\theta, \mathbf{v}_\phi)$ is some predefined velocity field with azimuthal and polar components $\mathbf{v}_\theta$ and $\mathbf{v}_\phi$, respectively. We considered a unidirectional profile $\mathbf{v}_\theta = \xi \sin\theta$ and $\mathbf{v}_\phi = 0$, where ξ is a constant. This flow profile is strongest near the equator and vanishes near the poles. In the regime of fast cytoplasmic diffusion, this leads to the modified version of Equation (7):

$$\frac{\partial u}{\partial \tau} = \delta^2 \left(\frac{1}{\sin\theta} \frac{\partial}{\partial \theta} \left(\sin\theta \frac{\partial u}{\partial \theta} \right) + \frac{1}{\sin^2\theta} \frac{\partial^2 u}{\partial \phi^2} \right) - \frac{\epsilon}{\sin\theta} \frac{\partial \left(u \sin^2\theta \right)}{\partial \theta} + \left(1 - \frac{\alpha}{2\pi} \int_0^{2\pi} \int_0^{\pi} u \sin\theta \, \mathrm{d}\theta \, \mathrm{d}\phi \right) \left(\beta + \frac{u^\nu}{u^\nu + \gamma^\nu} \right) - u. \tag{S92}$$

The new dimensionless group, $\epsilon \equiv \xi/(k_d r)$, can be interpreted as the ratio of the time scale of dissociation from the membrane and the time scale of convective transport along the surface. Transient flow that is present only during the finite time window $\tau \in [0, \tau_c]$ is modeled by multiplying the new term by a Heaviside function:

$$\frac{\partial u}{\partial \tau} = \delta^2 \left(\frac{1}{\sin\theta} \frac{\partial}{\partial \theta} \left(\sin\theta \frac{\partial u}{\partial \theta} \right) + \frac{1}{\sin^2\theta} \frac{\partial^2 u}{\partial \phi^2} \right) - \frac{\epsilon}{\sin\theta} \frac{\partial \left(u \sin^2\theta \right)}{\partial \theta} H(\tau_c - \tau) + \left(1 - \frac{\alpha}{2\pi} \int_0^{2\pi} \int_0^{\pi} u \sin\theta \, \mathrm{d}\theta \, \mathrm{d}\phi \right) \left(\beta + \frac{u^\nu}{u^\nu + \gamma^\nu} \right) - u. \tag{S93}$$

Equation (S93) was solved using Chebfun, as described above. In Figure 4 of the main text, the spherical cap was formed for $\epsilon = 1$ and $\tau_c = 2$ from an initially homogeneous profile, with $(\alpha, \beta, \gamma, \delta^2) = (1, 0.1, 0.35, 0.05)$ in the regime $\nu \gg 1$.

Supporting References

[1] M. Abramowitz and I. Stegun, *(eds.): Handbook of mathematical functions,* National Bureau of Standards (1964).

[2] B. S. Kerner and V.V. Osipov, *Autosolitons,* Kluwer, Dordrecht (1994).

[3] B. S. Kerner and V.V. Osipov, *Nonlinear theory of stationary strata in dissipative systems,* Sov. Phys. - JETP, 47 (1978), pp. 874 - 885.

[4] B. S. Kerner and V.V. Osipov, *Pulsating "heterophase" regions in nonequilibrium systems,* Sov. Phys. - JETP, 56 (1982), pp. 1275 - 1282.

[5] C. B. Muratov and V.V. Osipov, *General theory of instabilities for patterns with sharp interfaces in reaction-diffusion systems,* Phys. Rev. E, 53 (1996), pp. 3101-3116.

[6] A. Bose and G. A. Kriegsmann, *Stability of localized structures in non-local reaction-diffusion equations,* Meth. Appl. Anal., 5 (1998), pp. 351-366.

[7] C. B. Muratov and V.V. Osipov, *Stability of static spike autosolitons in the Gray-Scott model.* SIAM J. Appl. Math., 62 (2002), pp. 1463 - 1487.

[8] B. Klünder, T. Freisinger, R. Wedlich-Söldner, and E. Frey, *GDI-mediated cell polarization in yeast provides precise spatial and temporal control of Cdc42 signaling.* PLoS Comput. Biol., 9 (2013), 1003396.

[9] H. Montanelli and Y. Nakatsukasa, *Fourth-order time-stepping for stiff PDEs on the sphere,* SIAM J. Sci. Comput., 40 (2018), pp. A421-A451.

[10] S. Filip, A. Javeed, and L. N. Trefethen, *Smooth random functions, random ODEs, and Gaussian processes,* SIAM Rev. (submitted).